Asia Pac. J. Math. 2026 **13**:86

A BEHAVIOR–CLIMATE COUPLED SIR MODEL FOR DENGUE TRANSMISSION: A DATA-DRIVEN APPROACH FOR BANGLADESH

MD MASHUD PARVEZ[1,*], MD IBRAHIM KHOLIL[2], DANIYAL-UR-REHMAN[3], BALAL AALAM[4]

[1]Department of Mathematics, Dhaka University of Engineering and Technology, Gazipur, 1707, Bangladesh

[2]Department of Mathematics, Norfolk State University, Norfolk, VA 23504, United States

[3]Department of Computer Science, IQRA University, Karachi, PK 75300, Pakistan

[4]Department of Mathematics, School of Science, King Mongkut's Institute of Technology Ladkrabang, Bangkok, 10520, Thailand

[*]Corresponding author: mmparvez@duet.ac.bd

Received Mar. 2, 2026

Abstract. We investigate the joint roles of climate variability and human preventive behavior in dengue transmission in Bangladesh by developing a Behavior–Climate Coupled Susceptible–Infected–Recovered (BC–SIR) model. The model integrates a climate suitability index derived from rainfall and temperature with a behavioral compliance variable that represents both adoption and fatigue of preventive actions. The transmission rate is jointly modulated by climate and behavior, enabling data-informed parameter estimation. We establish positivity and boundedness of solutions, derive the basic reproduction number $\mathscr{R}_0$, and analyze the local stability of the disease-free equilibrium. Sensitivity analysis identifies climate suitability and behavioral efficacy as key drivers of transmission intensity. Numerical experiments indicate that sustained behavioral adherence can substantially mitigate outbreaks even under favorable climatic conditions. The BC–SIR framework provides a flexible basis for incorporating environmental and behavioral factors into dengue control strategies.

2020 Mathematics Subject Classification. 92D30; 62P10; 65L06; 37N25.

Key words and phrases. dengue transmission; behavior–climate SIR model; climate suitability; mathematical epidemiology; Bangladesh.

1. Introduction

Dengue remains one of the most significant mosquito-borne viral diseases in tropical and subtropical regions, causing more than 400 million infections annually worldwide [8, 30]. In Bangladesh, dengue has transitioned from a sporadic to a hyperendemic disease, with outbreaks showing a strong seasonal pattern linked to monsoon rainfall and temperature [21]. The country has experienced record-breaking epidemics in recent years, highlighting the need for predictive and adaptive models that incorporate

DOI: 10.28924/APJM/13-86

both climatic and behavioral determinants of disease transmission. Rainfall, temperature, and humidity modulate the abundance, biting rate, and survival of *Aedes aegypti* mosquitoes—the primary vector of dengue virus—while human behaviors such as source reduction, repellent use, and early treatment-seeking significantly modify exposure and infection risk [17, 19]. Understanding how these environmental and behavioral factors interact is essential for effective outbreak prediction and public health response.

Classical SIR-type epidemic models [5] have long been used to capture infectious disease dynamics, including dengue [29, 32, 38]. However, many of these models assume a fixed or seasonally forced transmission rate, which limits their ability to account for dynamic feedback between climate variability and adaptive human responses. Recent advances in mechanistic and data-driven modeling demonstrate that climatic factors such as rainfall and temperature influence dengue transmission with lag effects of several weeks [20, 21, 24]. At the same time, behavioral adaptation—driven by public awareness, risk perception, and government campaigns—can alter human–vector contact patterns over time [6, 17, 19]. Models that ignore this feedback risk systematic underestimation of epidemic peaks and timing.

In Bangladesh, a growing body of research has investigated the climate–dengue nexus through statistical, spatial, and machine-learning frameworks. For instance, [2] proposed a climate-driven SIR model calibrated with rainfall and temperature data, while [31] and [4] used autoregressive and time-series models to forecast dengue incidence from 2008–2024. Spatial analyses by [37] and [33] revealed clustering of dengue hot spots in Dhaka and Chittagong, strongly correlated with urbanization and precipitation patterns. Furthermore, [35] applied explainable artificial intelligence (XAI) to identify key eco-climatic predictors of dengue outbreaks, underscoring the increasing role of data-driven approaches in Bangladesh. Globally, the predictive capabilities of climate-based dengue models have been enhanced through ensemble and superensemble frameworks such as those developed by [45], [38], and [29]. These models integrate multiple climatic inputs and provide probabilistic forecasts of epidemic intensity, yet they seldom incorporate behavioral adaptation explicitly.

In addition to climatic influences, behavioral factors have a measurable effect on dengue transmission dynamics. Studies in Bangladesh indicate significant variability in public awareness, knowledge, and preventive practices [6, 19]. Despite widespread awareness campaigns, fatigue in preventive behavior often emerges after outbreak peaks, highlighting the temporal dynamics of human compliance. Traditional compartmental models rarely account for these psychological and social processes. The few studies that link behavioral adaptation with infectious disease dynamics (e.g., [17]) emphasize that neglecting behavioral change can lead to substantial model misspecification and forecasting errors.

To address these gaps, we develop a parsimonious *Behavior–Climate Coupled Susceptible–Infected–Recovered* (*BC–SIR*) model tailored to dengue transmission in Bangladesh. The framework integrates two key drivers of transmission dynamics: (i) a climate suitability index $V(t)$ derived from rainfall and

temperature time series incorporating empirically justified lag structures, and (ii) a behavioral compliance variable $B(t) \in [0, 1]$ that captures the evolving level of individual and community adherence to preventive practices such as source reduction, household screening, repellant use, and early care-seeking. The force of infection is therefore modulated jointly by exogenous environmental conditions and endogenous behavioral responses, allowing the model to represent how populations adjust their preventive actions in response to perceived and actual disease risk. By calibrating this system against weekly epidemiological data from DGHS/IEDCR and meteorological records from BMD, the BC–SIR model provides a transparent, data-driven representation of dengue transmission dynamics that is suitable for short-term forecasting, retrospective outbreak interpretation, and forward-looking policy evaluation under alternative climatic and behavioral scenarios.

Existing climate-driven dengue models commonly treat human behavior either as constant over time or as an externally specified input, independent of disease prevalence. Such formulations overlook the well-documented adaptive nature of protective behavior, whereby individuals modify preventive actions in response to perceived infection risk, public health messaging, and social reinforcement. By contrast, our BC–SIR framework incorporates behavioral adaptation explicitly within the transmission mechanism, allowing $B(t)$ to respond dynamically to epidemiological conditions while also decaying in the absence of persistent motivation or risk cues. In parallel, the climate suitability index $V(t)$ is grounded in observable meteorological processes and captures environmentally mediated variation in vector abundance and viral replication. This explicit coupling of climate forcing and adaptive behavior results in a nonlinear feedback system capable of reproducing complex, empirically observed outbreak patterns. To the best of our knowledge, this is the first modeling framework developed specifically for Bangladesh that jointly quantifies climate suitability and behavioral compliance within a unified dynamic system. As such, the BC–SIR model offers new insight into climate-sensitive and community-centered dengue control strategies, with implications for public health planning, risk communication, and targeted intervention timing.

2. Behavior–Climate Coupled SIR (BC–SIR) Model

2.1. **Model Structure and Definitions.**

We consider a compartmental model describing dengue transmission among the human population, incorporating demographic processes, temporary immunity, behavioral compliance, and climate suitability for transmission. Let $S(t)$, $I(t)$, and $R(t)$ denote the numbers of *susceptible*, *infectious*, and *recovered* (*temporarily immune*) individuals, respectively, at time t. The total human population is therefore

$$N(t) = S(t) + I(t) + R(t).$$

Two additional auxiliary variables modulate transmission dynamics. The quantity $B(t) \in [0, 1]$ repre-

sents the level of behavioral compliance, where $B = 0$ corresponds to complete noncompliance (no preventive behavior) and $B = 1$ to full compliance (complete adherence to preventive measures such as using repellents or removing stagnant water). The variable $V(t) \geq 0$ quantifies the suitability of the climate for mosquito-mediated transmission, incorporating the effects of temperature, rainfall, and humidity.

Force of infection. The rate at which susceptible individuals become infected is determined by the *force of infection* $\lambda(t)$, which depends on both climate suitability and behavioral compliance. Specifically,

$$\lambda(t) = \Big[\beta\, V(t)\,\big(1 - \varepsilon B(t)\big) + \beta_0\Big]\frac{I(t)}{N(t)}, \tag{1}$$

where $\beta > 0$ is the climate-amplified transmission rate, $\varepsilon \in [0, 1]$ measures the effectiveness of behavior in reducing transmission, and $\beta_0 \geq 0$ represents a small background transmission component independent of climate or behavior.

Equation (1) defines the force of infection $\lambda(t)$, representing the per capita rate at which susceptible individuals acquire infection. The transmission process is governed by three interacting components: climate-driven suitability $V(t)$, behavioral compliance $B(t)$, and the proportion of infectious individuals $\frac{I(t)}{N(t)}$. The term $\beta V(t)$ denotes the effective contact rate modulated by climatic factors such as rainfall and temperature, which influence mosquito density and biting frequency. The behavioral adjustment factor $(1-\varepsilon B(t))$ reduces transmission according to the level of compliance $B(t) \in [0, 1]$ and the efficacy parameter $\varepsilon \in [0, 1]$. When $B(t) = 0$, no preventive behavior is adopted. When $B(t) = 1$ with $\varepsilon = 1$, the climate-driven component of transmission is maximally suppressed, leading to a *strong reduction* in the force of infection rather than a complete interruption, since $\lambda(t)$ remains influenced by the baseline transmission rate β_0. The additive constant β_0 accounts for residual transmission or importation that persists independently of climate conditions and behavioral compliance. Consequently, the structure of (1) ensures that $\lambda(t)$ responds smoothly and realistically to variations in both climate and population behavior.

Behavioral dynamics. Behavioral compliance is influenced by both external campaigns and perceived disease risk. Its evolution is modeled as

$$\frac{dB}{dt} \;=\; \alpha_0(1 - B) \;+\; \alpha\,\frac{I}{N}\,(1 - B) \;-\; \eta\, B, \tag{2}$$

where $\alpha_0 \geq 0$ is the rate of spontaneous adoption of preventive behaviors due to awareness campaigns, $\alpha \geq 0$ quantifies the reactive (risk-driven) increase in compliance when infection prevalence rises, and $\eta \geq 0$ represents behavioral fatigue or waning of compliance over time.

Equation (2) models the temporal evolution of behavioral compliance $B(t)$. The first term, $\alpha_0(1 - B)$, represents spontaneous or campaign-driven adoption of preventive measures, acting independently of current infection levels. The second term, $\alpha\,\frac{I}{N}(1 - B)$, captures reactive adoption, whereby individuals increase compliance in response to heightened disease prevalence. Both processes are saturating,

as indicated by the factor $(1 - B)$, which prevents $B(t)$ from exceeding unity. The final term, $-\eta B$, accounts for behavioral fatigue or waning adherence over time. The formulation guarantees that $B(t)$ remains bounded in $[0, 1]$ and captures realistic social dynamics in which preventive behavior increases under risk but gradually decays in the absence of reinforcement. Similar functional forms have been employed in behavioral–epidemiological models to represent adaptive human responses to infection risk [12, 15, 17].

Climate suitability. The climate suitability index $V(t)$ captures environmental drivers such as rainfall and temperature, which influence mosquito abundance and virus replication. In applications, $V(t)$ can be derived directly from meteorological data or modeled dynamically. A simple dynamic representation is

$$\frac{dV}{dt} = -\xi V + \xi_r \mathcal{R}(t - \tau_r) + \xi_t \mathcal{T}(t - \tau_t), \tag{3}$$

where $\mathcal{R}(t)$ and $\mathcal{T}(t)$ denote normalized rainfall and temperature indices, respectively, τ_r and τ_t are corresponding lag times, and $\xi, \xi_r, \xi_t \geq 0$ are rate constants governing the responsiveness of $V(t)$ to climatic inputs.

Equation (3) characterizes the temporal evolution of the climate suitability index $V(t)$, which encapsulates environmental drivers such as rainfall and temperature that influence mosquito abundance, biting activity, and viral replication rates. The first term, $-\xi V$, represents the natural decay of climatic influence over time, ensuring that $V(t)$ relaxes toward zero in the absence of favorable conditions. The second and third terms, $\xi_r \mathcal{R}(t - \tau_r)$ and $\xi_t \mathcal{T}(t - \tau_t)$, describe the delayed contributions of rainfall and temperature, respectively, with lag parameters τ_r and τ_t accounting for ecological delays in mosquito population and virus dynamics. The coefficients ξ_r and ξ_t control the relative importance of rainfall and temperature in modulating transmission potential, while ξ governs the overall responsiveness or "memory" of the system to climatic forcing. When meteorological data are available, $V(t)$ may be derived empirically as a normalized function of observed rainfall and temperature, whereas the dynamic formulation in (3) offers a convenient low-dimensional representation for simulation and forecasting purposes. This approach parallels earlier efforts to couple vector-borne disease models with climatic drivers through lagged or smoothed environmental indices (see, e.g., [8, 18, 23]).

2.2. **Flow Chart and Model.** Illustrate a flow chart of individuals among the susceptible, infectious, and recovered compartments in the BC–SIR framework. Susceptible individuals $S(t)$ become infected at a rate determined by the force of infection, which is jointly influenced by climate suitability $V(t)$ and behavioral compliance $B(t)$. Higher climate suitability, reflecting favorable rainfall and temperature conditions, enhances mosquito abundance and viral transmission efficiency, thereby increasing the likelihood of infection. Conversely, greater behavioral compliance—including practices such as source reduction, household screening, and personal protection—reduces the effective contact rate between

humans and mosquitoes, thus lowering transmission potential. Once infected, individuals transition into the infectious compartment $I(t)$, where they contribute to further transmission until recovery. Recovered individuals $R(t)$ acquire temporary immunity before gradually returning to the susceptible pool due to waning immunity.

Importantly, empirical studies have shown that preventive behaviors in dengue-endemic settings are not static but evolve dynamically in response to perceived risk, public health messaging, and local outbreak intensity [3, 15, 17]. This motivates the explicit inclusion of $B(t)$ as a behavioral adaptation variable within the transmission mechanism. The flow structure therefore captures both climate-driven increases in transmission risk and behavior-driven mitigation efforts that emerge from community awareness and intervention campaigns.

A complete description of the model parameters is provided in Table 1, and the governing system of differential equations formalizing these transitions is presented in the following:

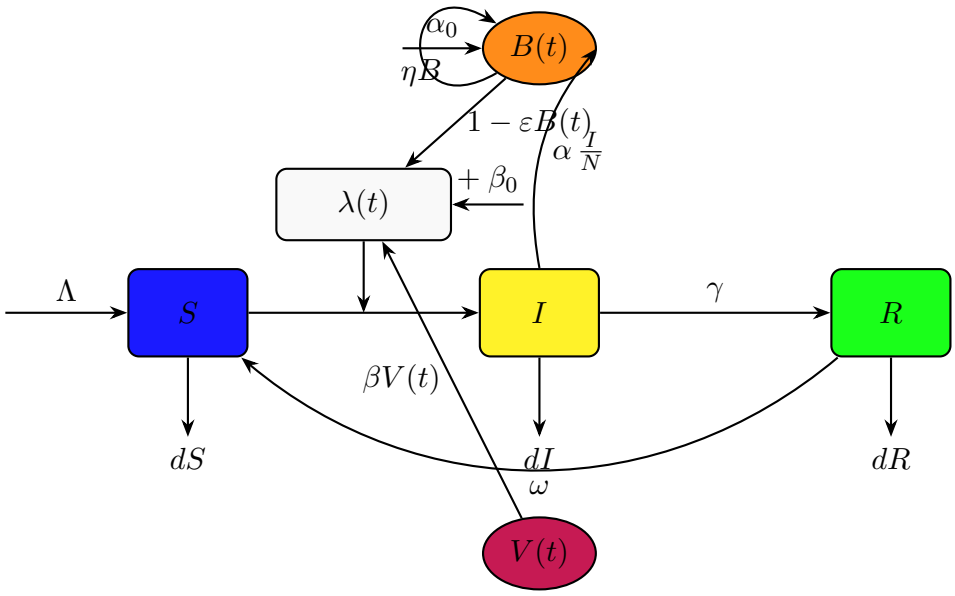

Figure A. Human SIR with behavior $B(t)$ and climate suitability $V(t)$ modulating the force of infection $\lambda(t)$.

Parameters	**The Physical Representation**	**Values**	**Units**	**Reference**
Λ	Recruitment rate	$10,000$	persons/day	[41,42]
d	Natural death rate	0.001	1/day	[22]
β	Climate-amplified transmission scale	0.90	1/day	[28,30]
β_0	Background transmission	0.25	1/day	[46]
γ	Recovery rate	0.1428	1/day	[1,43]
ω	Waning immunity rate	0.0055	1/day	[25]
ε	Behavior efficacy	0.55	—	[6,19]
$V(t)$	Climate suitability	0.7	—	[13,27]
ξ, ξ_r, ξ_t	Climate filter gains	$0.5, 0.6, 0.4$	1/day	[11,29,36]
τ_r, τ_t	Climate lags	$30, 0$	days	[27,44]
α_0	Spontaneous adoption	0.01	1/day	[16,34]
α	Reactive adoption	1.80	1/day	[17,34]
η	Behavioral fatigue	0.07	1/day	[7]

TABLE 1. Parameter values and descriptions.

2.3. **The BC–SIR Model.** The human population is divided into susceptible $S(t)$, infectious $I(t)$, and recovered $R(t)$ individuals. The behavior compliance level is denoted by $B(t) \in [0,1]$. Population turnover, infection, recovery, behavioral adaptation, and immunity waning are represented in the following system:

$$\frac{dS}{dt} = \Lambda - \lambda(t)\, S - dS + \omega R, \tag{4}$$

$$\frac{dI}{dt} = \lambda(t)\, S - (\gamma + d)I, \tag{5}$$

$$\frac{dR}{dt} = \gamma I - (\omega + d)R, \tag{6}$$

$$\frac{dB}{dt} = \alpha_0(1 - B) + \alpha \frac{I}{N}(1 - B) - \eta B \tag{7}$$

where $N(t) = S + I + R$ and the force of infection is

$$\lambda(t) = \big[\beta V(t)\big(1 - \varepsilon B(t)\big) + \beta_0\big]\,\frac{I(t)}{N(t)}. \tag{8}$$

3. Mathematical Analysis of the BC–SIR System

In this section, we analyze the dynamical properties of the BC–SIR system in 2.3 with the force of infection defined in (8). We assume $V(t)$ is bounded and nonnegative. For equilibrium and stability analysis, we consider the special case $V(t) = \bar{V}$ and denote $B(t)$ by its equilibrium value B^* when appropriate.

For analytical tractability, the climate suitability index $V(t)$ is treated as a constant $\bar{V}$ at equilibrium, and the behavioral compliance dynamics are evaluated at the behavioral steady state B^*. Under these assumptions, the force of infection reduces to

$$\lambda^* = \frac{\beta\,\bar{V}\,(1 - \varepsilon B^*) + \beta_0}{N}\,I,$$

which is used in deriving reproduction number $\mathscr{R}_0$ and stability conditions.

Before proceeding with equilibrium and stability analysis, we first verify that the BC–SIR system is mathematically well-posed. In particular, we show that the solutions remain nonnegative and biologically meaningful for all time, and that the total population remains uniformly bounded. The next theorem confirms that this property holds and that the system is well-posed in the biologically feasible region.

Theorem 1. *Let the initial data satisfy*

$$S(0) \geq 0, \qquad I(0) \geq 0, \qquad R(0) \geq 0, \qquad B(0) \in [0, 1].$$

Then the solution of (4)–(7) *exists for all* $t \geq 0$, *satisfies*

$$S(t), I(t), R(t) \geq 0 \quad \textit{for all } t \geq 0, \qquad B(t) \in [0, 1] \textit{ for all } t \geq 0,$$

and, if $d > 0$, *the total population obeys*

$$N(t) \leq \frac{\Lambda}{d} + \Big(N(0) - \frac{\Lambda}{d}\Big)e^{-dt},$$

so $\limsup_{t\to\infty} N(t) \leq \dfrac{\Lambda}{d}$.

Proof. Write $X = (S, I, R, B)^\top$ and $\dot{X} = F(X, t)$ where F is given by the right-hand sides of (4)–(7). Since $V(t)$ is assumed bounded and

$$\lambda(t) = \big(\beta V(t)(1 - \varepsilon B) + \beta_0\big)\frac{I}{N}$$

is continuous on $\{(S, I, R, B) : S \geq 0, I \geq 0, R \geq 0, N > 0, B \in \mathbb{R}\}$ and locally Lipschitz away from $N = 0$, the Picard–Lindelöf theorem guarantees a unique maximal solution $X(t)$ on some interval $[0, T_{\max})$.

We show that $S(t), I(t), R(t) \geq 0$ on $[0, T_{\max})$. Suppose there exists $t_* \in [0, T_{\max})$ such that $S(t_*) = 0$. Then, from (4),

$$\dot{S}(t_*) = \Lambda - \lambda(t_*) \cdot 0 - d \cdot 0 + \omega R(t_*) = \Lambda + \omega R(t_*) \geq 0,$$

since $\Lambda \geq 0$ and $R(t_*) \geq 0$. Hence $S(t)$ cannot cross from nonnegative to negative values, and therefore $S(t) \geq 0$ for all $t \in [0, T_{\max})$.

For I, from (5)

$$\dot{I} = \lambda S - (\gamma + d)I \geq -(\gamma + d)I,$$

so comparison with $\dot{y}_I = -(\gamma + d)y_I$, $y_I(0) = I(0) \geq 0$, yields $I(t) \geq y_I(t) \geq 0$ on $[0, T_{\max})$.

For R, (6) gives

$$\dot{R} = \gamma I - (\omega + d)R \geq -(\omega + d)R,$$

and comparison with $\dot{y}_R = -(\omega + d)y_R$, $y_R(0) = R(0) \geq 0$, yields $R(t) \geq y_R(t) \geq 0$.

Thus S, I, R remain nonnegative on $[0, T_{\max})$.

Consider $\dot{B} = \alpha_0(1 - B) + \alpha \frac{I}{N}(1 - B) - \eta B$. Since $I/N \geq 0$, we have for any $t \in [0, T_{\max})$:

$$\dot{B} \geq \alpha_0(1 - B) - \eta B = \alpha_0 - (\alpha_0 + \eta)B.$$

We define $u(t)$ as the solution of the linear ODE

$$\dot{u} = \alpha_0 - (\alpha_0 + \eta)u, \qquad u(0) = B(0).$$

The solution for the above ODE

$$u(t) = \frac{\alpha_0}{\alpha_0 + \eta} + \Big(B(0) - \frac{\alpha_0}{\alpha_0 + \eta}\Big)e^{-(\alpha_0 + \eta)t},$$

and in particular $u(t) \in \mathbb{R}$. By comparison, $B(t) \geq u(t)$ while the coefficients are defined. Evaluate the sign at the lower boundary: if $B(0) \geq 0$ then $u(t) \geq 0$ for all $t \geq 0$, hence $B(t) \geq 0$.

Similarly, because $I/N \geq 0$,

$$\dot{B} \leq \alpha_0(1 - B) + \alpha(1 - B) - \eta B = (\alpha_0 + \alpha) - (\alpha_0 + \alpha + \eta)B.$$

Let $v(t)$ solve

$$\dot{v} = (\alpha_0 + \alpha) - (\alpha_0 + \alpha + \eta)v, \qquad v(0) = B(0),$$

whose solution satisfies $v(t) \leq 1$ whenever $B(0) \leq 1$. By comparison, $B(t) \leq v(t) \leq 1$. Combining the two inequalities yields $B(t) \in [0, 1]$ for all $t \in [0, T_{\max})$.

Adding (4)–(6) yields the linear scalar ODE

$$\dot{N} = \Lambda - dN.$$

For $d \neq 0$, we have

$$N(t) = N(0)e^{-dt} + \frac{\Lambda}{d}\big(1 - e^{-dt}\big),$$

and hence, for all $t \in [0, T_{\max})$,

$$N(t) \le \frac{\Lambda}{d} + \Big(N(0) - \frac{\Lambda}{d}\Big)e^{-dt}.$$

In particular, if $d > 0$, then $N(t)$ is bounded on $[0, T_{\max})$, and since $0 \le S(t), I(t), R(t) \le N(t)$ and $B(t) \in [0, 1]$, the solution remains in a bounded subset of the domain of F on any finite time interval. Therefore, by the standard ODE continuation (extension) theorem, we must have $T_{\max} = \infty$. Consequently, the above estimate holds for all $t \ge 0$, and taking $\limsup_{t\to\infty}$ gives

$$\limsup_{t\to\infty} N(t) \le \frac{\Lambda}{d}.$$

Thus, we have uniform bounds on each component on any finite time interval:

$$\mathcal{D} = \{\, 0 \le S,\, I,\, R \le \max\{N(0),\, \Lambda/d\}, \quad B \in [0, 1] \,\}.$$

Hence, the solution remains in a compact subset of the domain of F for all finite time, preventing finite-time blow-up. Standard ODE extension theorems therefore imply $T_{\max} = \infty$, i.e., the solution exists for all $t \ge 0$. □

3.1. **Basic Reproduction Number.** Although the BC–SIR system 2.3 is four-dimensional, only the infected compartment $I(t)$ contributes to the generation of new infections. The variables $S(t)$ and $R(t)$ represent non–infectious population groups, while $B(t) \in [0, 1]$ is a dimensionless behavioral compliance level and does not represent a population subclass. The behavioral variable modulates transmission through the factor $1 - \varepsilon B(t)$, but it does not produce new infections itself. Therefore, in the next-generation formulation [39], only the infected subsystem is considered. In particular, the infected subspace is one–one-dimensional, so the next–generation matrix reduces to a 1×1 scalar. We will include $B(t)$ in the Jacobian matrix because it is a dynamic state variable, but we will not include it in the infected subsystem because it does not generate new infections.

Let the state vector be $x = (S, I, R, B)^\top$. Take the disease-free equilibrium

$$x_0 = (S^*, I^*, R^*, B^*) = \Big(N,\ 0,\ 0,\ B^*\Big), \qquad B^* = \frac{\alpha_0}{\alpha_0 + \eta}, \qquad N = \frac{\Lambda}{d},$$

and denote a representative (constant) climate level by $\bar{V}$ when required.

Define the new-infection vector $\mathscr{F}(x)$ and the transition/removal vector $\mathscr{V}(x)$ by

$$\mathscr{F}(x) = \begin{pmatrix} 0 \\ \big[\beta\,\bar{V}\,(1 - \varepsilon B) + \beta_0\big]\dfrac{I}{N}\,S \\ 0 \\ 0 \end{pmatrix}, \qquad \mathscr{V}(x) = \begin{pmatrix} -\Lambda + \lambda S + dS - \omega R \\ (\gamma + d)I \\ -\gamma I + (\omega + d)R \\ -\alpha_0(1 - B) - \alpha\dfrac{I}{N}(1 - B) + \eta B \end{pmatrix},$$

where $\lambda = \big[\beta\,\bar{V}(1 - \varepsilon B) + \beta_0\big]\dfrac{I}{N}$.

Linearize at x_0, the Jacobians $F = D\mathscr{F}(x_0)$ and $V = D\mathscr{V}(x_0)$ are

$$F = D\mathscr{F}(x_0) = \begin{pmatrix} 0 & 0 & 0 & 0 \\ 0 & c & 0 & 0 \\ 0 & 0 & 0 & 0 \\ 0 & 0 & 0 & 0 \end{pmatrix}, \qquad c := \beta \bar{V} (1 - \varepsilon B^*) + \beta_0,$$

and

$$V = D\mathscr{V}(x_0) = \begin{pmatrix} \beta_0 + d & -c & 0 & \omega \\ 0 & \gamma + d & 0 & 0 \\ 0 & -\gamma & \omega + d & 0 \\ 0 & -\frac{\alpha}{N}(1 - B^*) & 0 & \alpha_0 + \eta \end{pmatrix}.$$

(Entries follow from differentiation of the right-hand sides; the only new-infection term appears in the I-equation.)

Because the infected subspace here is one-dimensional (the single infectious compartment I), we extract the infected block matrices as scalars:

$$F_{(I)} = [\, c \,], \qquad V_{(I)} = [\, \gamma + d \,],$$

so the next-generation matrix (infected-subsystem) is

$$K = F_{(I)} V_{(I)}^{-1} = \frac{c}{\gamma + d}.$$

Hence, the basic reproduction number at the DFE is the spectral radius of K can be written explicitly as

$$\mathscr{R}_0 = \rho(K) = \frac{\beta \bar{V} (1 - \varepsilon B^*) + \beta_0}{\gamma + d}.$$

Utilizing equation (14) from the sensitivity analysis, we determine the most sensitive parameters for $\mathscr{R}_0$. The following three-dimensional surfaces show how the fundamental reproduction number $\mathscr{R}_0$. The fluctuates with the most significant factors found by the sensitivity analysis: behavioral factor (ε), transmission rate (β), recovery rate (γ), and vaccination rate ($\overline{V}$). The surface exhibits a significant positive dependence on $\mathscr{R}_0$.

When the transmission rate β and the effective contact factor $\overline{V}$ rise, $\mathscr{R}_0$ increases rapidly, suggesting that increased behavioral exposure or transmission may significantly accelerate the spread of disease, and the second plot shows that $\mathscr{R}_0$ increases linearly. The highlighting the fact that weaker preventative behavior (ε) and increased transmission efficiency work together to increase the risk of infection, as shown in Figure (1). This surface highlights a nonlinear interaction on $\mathscr{R}_0$. When the recovery rate γ is poor, it increases rapidly for high transmission rates β, but when the recovery improves, it decreases sharply. It demonstrates that the equilibrium between the dynamics of infection and recovery plays

(A) Effect of $(\beta, \overline{V})$ on $\mathscr{R}_0$. (B) Effect of (β, ε) on $\mathscr{R}_0$.

FIGURE 1. Sensitivity of $\mathscr{R}_0$ to climate and behavioral parameters.

(A) Effect of (β, γ) on $\mathscr{R}_0$. (B) Effect of $(\gamma, \overline{V})$ on $\mathscr{R}_0$.

FIGURE 2. Sensitivity of $\mathscr{R}_0$ to recovery and climate parameters.

a crucial role in determining the persistence of epidemics, and in the second graph $\mathscr{R}_0$ decreases dramatically as recovery rate γ increases, whereas rising $\overline{V}$ increases $\mathscr{R}_0$. This illustrates how recovery and epidemic potential are inversely correlated; quicker recovery results in shorter infectious periods and, hence, lower epidemic potential, as seen in Figure (2).

3.2. **Nonautonomous next-generation and the effective reproduction number.** When climate suitability and behaviour are time-dependent, i.e. $V = V(t)$ and $B = B(t)$, the model is nonautonomous and the transmission coefficient becomes time-varying:

$$c(t) \;:=\; \beta\, V(t)\,\big(1 - \varepsilon B(t)\big) + \beta_0.$$

Two useful time-dependent reproduction quantities are the *instantaneous reproduction potential* and the effective reproduction number. Formally linearizing the model at time t about the disease-free state (holding $S \approx N$) yields the instantaneous next–generation scalar

$$K_{\text{inst}}(t) \;=\; \frac{c(t)}{\gamma + d}.$$

We call $K_{\text{inst}}(t)$ the *instantaneous reproduction potential* (it is the analogue of $\mathscr{R}_0$ with parameters frozen at time t). Accounting for the current susceptible fraction $S(t)/N(t)$ gives the time-dependent effective reproduction number

$$\mathscr{R}_t \;=\; \frac{c(t)}{\gamma + d}\,\frac{S(t)}{N(t)} \;=\; \frac{\beta\, V(t)\,(1 - \varepsilon B(t)) + \beta_0}{\gamma + d}\,\frac{S(t)}{N(t)}. \tag{9}$$

If $\mathscr{R}_t > 1$ (and remains so over a time window comparable to the generation interval), the number of new infections will tend to increase at time t; conversely, if $\mathscr{R}_t < 1$ infections tend to decline. $\mathscr{R}_t$ is a local (in time) threshold: for nonautonomous systems it is not a global bifurcation parameter—transient growth can occur even if the time-average of $\mathscr{R}_t$ is below one, particularly under strong seasonality. When $V(t), B(t)$ are periodic (e.g. annual monsoon forcing) a more precise long-term threshold is given by the dominant Floquet multiplier of the linearized periodic system or by the spectral radius of a period-advancement operator (see below).

A more mechanistic representation uses the renewal (Volterra) formulation. Let $w(s)$ denote the generation-interval distribution (infectivity profile of an index case of age s). Then the incidence $i(t)$ satisfies approximately

$$i(t) \;=\; \int_0^\infty i(t-s)\, \underbrace{\Big(\frac{S(t)}{N(t)}\, c(t)\, w(s)\Big)}_{=\,K(t,s)}\, ds,$$

where $K(t,s)$ is the time-varying infectivity kernel (new infections at time t produced by cases of infection-age s. Under this renewal formulation one can define the time-varying reproduction number [40] [14] as

$$\mathscr{R}_t^{(\text{renewal})} \;=\; \frac{i(t)}{\displaystyle\int_0^\infty i(t-s)\, w(s)\, ds}\,,$$

or, equivalently for a separable kernel,

$$\mathscr{R}_t^{(\text{renewal})} \approx \frac{c(t)}{\gamma + d}\frac{S(t)}{N(t)}$$

when $w(s)$ has mean $1/(\gamma + d)$. Thus the instantaneous algebraic formula (9) coincides with the renewal-based definition under the usual assumptions about the generation interval.

Remark 1. *Equation* (9) *gives the* instantaneous *or* time-varying *reproduction number appropriate for real-time monitoring. The* case *reproduction number* (*Wallinga–Teunis*) [40] *measures the average number of secondary cases caused by an individual infected at time t and requires reconstructing transmission pairs or using the generation-interval distribution. If $V(t), B(t)$ are strictly periodic with period T, then the long-term threshold for persistence is determined by the spectral radius of the period-map* (*or the principal Floquet multiplier*) *of the linearized system rather than the instantaneous $\mathscr{R}_t$. Numerically one computes the principal multiplier by integrating the linearized system over one period and taking the dominant eigenvalue. In practice $\mathscr{R}_t$ (eq.* (9)) *is useful for short-term situational awareness* (*is transmission rising or falling today?*), *while the Floquet/renewal approaches are needed to assess persistence and multi-year patterns under strong seasonality. The algebraic form $\mathscr{R}_t = c(t)/(\gamma + d) \cdot S(t)/N(t)$ is exact for the SIR-type model with homogeneous mixing and exponentially distributed infectious period. For more structured or stochastic models, or when the generation-interval has a different shape, substitute the appropriate mean generation interval in the renewal expression above.*

3.3. **Stability Analysis of the Equilibria.** We begin by examining the equilibrium structure of the autonomous BC–SIR system under the assumption that the climate variable V is frozen at a representative constant level $\bar{V}$ and that the behavioural variable B is held at its corresponding equilibrium value.

Disease–free equilibrium (DFE).. At the disease–free equilibrium, infection is absent and behaviour settles at

$$B_0 = \frac{\alpha_0}{\alpha_0 + \eta}.$$

The disease–free equilibrium state is therefore

$$x_0 = (S_0, I_0, R_0, B_0) = \left(\tfrac{\Lambda}{d},\, 0,\, 0,\, B_0\right).$$

Define the frozen transmission coefficient

$$c_0 := \beta\, \bar{V}\, (1 - \varepsilon B_0) + \beta_0,$$

and the corresponding basic reproduction number

$$\mathscr{R}_0 = \frac{c_0}{\gamma + d} = \frac{\beta\, \bar{V}\, (1 - \varepsilon B_0) + \beta_0}{\gamma + d}. \tag{10}$$

Endemic equilibrium (EE).. When $\mathscr{R}_0 > 1$, the model admits an endemic equilibrium

$$x_e = (S_e, I_e, R_e, B_e), \qquad I_e > 0,$$

obtained as a positive solution of the steady–state system

$$\begin{aligned} 0 &= \Lambda - \lambda_e S_e - d S_e + \omega R_e, \\ 0 &= \lambda_e S_e - (\gamma + d) I_e, \\ 0 &= \gamma I_e - (\omega + d) R_e, \\ 0 &= \alpha_0 (1 - B_e) + \alpha \frac{I_e}{N_e} (1 - B_e) - \eta B_e, \end{aligned} \tag{11}$$

where $N_e = S_e + I_e + R_e$ and

$$\lambda_e = \left[\beta\, \bar{V}\, (1 - \varepsilon B_e) + \beta_0\right] \frac{I_e}{N_e}.$$

These relations will be used in the subsequent stability analysis of the endemic equilibrium.

The Jacobian matrix of the vector field at the disease–free equilibrium (with the ordering $x = (S, I, R, B)$) is

$$J(x_0) = \begin{pmatrix} -d & -c_0 & \omega & 0 \\ 0 & c_0 - (\gamma + d) & 0 & 0 \\ 0 & \gamma & -(\omega + d) & 0 \\ 0 & \dfrac{\alpha(1 - B_0)}{N} & 0 & -(\alpha_0 + \eta) \end{pmatrix}. \tag{12}$$

The local dynamics near the disease–free equilibrium are governed by the eigenvalues of the Jacobian matrix (12). A direct spectral analysis yields the following result.

Theorem 2 (Local stability of the DFE)**.** *Let all parameters be nonnegative and $d > 0$. With $\mathscr{R}_0$ defined in (10), the disease–free equilibrium x_0 is locally asymptotically stable if $\mathscr{R}_0 < 1$ and unstable if $\mathscr{R}_0 > 1$. In particular,*

$$\operatorname{spec}\big(J(x_0)\big) = \Big\{\, c_0 - (\gamma + d),\ -d,\ -(\omega + d),\ -(\alpha_0 + \eta) \,\Big\}.$$

Proof. To expose the spectral structure it is convenient to permute the variables so that the infectious compartment I appears first. Permuting the ordering to $x' = (I, S, R, B)$ does not change the spectrum; under this ordering the matrix representation of $J(x_0)$ becomes

$$\widetilde{J}(x_0) = \begin{pmatrix} c_0 - (\gamma + d) & 0 & 0 & 0 \\ -\,c_0 & -d & \omega & 0 \\ \gamma & 0 & -(\omega + d) & 0 \\ \dfrac{\alpha(1 - B_0)}{N} & 0 & 0 & -(\alpha_0 + \eta) \end{pmatrix}.$$

Note that $\widetilde{J}(x_0)$ is block lower-triangular with blocks

$$\widetilde{J}(x_0) = \begin{pmatrix} A & 0 \\ C & D \end{pmatrix}, \qquad A = [\, c_0 - (\gamma + d) \,] \in \mathbb{R}^{1\times 1}, \quad D = \begin{pmatrix} -\,d & \omega & 0 \\ 0 & -(\omega + d) & 0 \\ 0 & 0 & -(\alpha_0 + \eta) \end{pmatrix}.$$

For block lower-triangular matrices the characteristic polynomial factors as the product of the characteristic polynomials of the diagonal blocks. Hence the eigenvalues of $\widetilde{J}(x_0)$ (and therefore of $J(x_0)$) are

$$\lambda_1 = c_0 - (\gamma + d), \qquad \lambda_2 = -d, \qquad \lambda_3 = -(\omega + d), \qquad \lambda_4 = -(\alpha_0 + \eta).$$

From these explicit eigenvalues the stability claim follows immediately. If $\mathscr{R}_0 < 1$, then by (10),

$$\lambda_1 = c_0 - (\gamma + d) = (\gamma + d)\big(\mathscr{R}_0 - 1\big) < 0,$$

and the remaining three eigenvalues are strictly negative because all parameters are nonnegative and $d > 0$. Therefore all eigenvalues have negative real part and the DFE is locally asymptotically stable.

Conversely, if $\mathscr{R}_0 > 1$ then $\lambda_1 > 0$, so the Jacobian has a positive eigenvalue and the DFE is unstable. □

Remark 2. *The factorization above shows that the only eigenvalue whose sign depends on disease transmission is λ_1. All other eigenvalues are strictly negative and determined by demographic, recovery, waning, and behavioral time scales; therefore, these terms do not generate instabilities of the DFE. The reproduction number $\mathscr{R}_0 = c_0/(\gamma + d)$ admits the usual interpretation: it is the expected number of secondary infections produced by a single*

infectious individual introduced into a wholly susceptible population when behaviour is held at its disease–free level B_0 and climate at the representative level $\bar{V}$.

For the full time-varying model (with $V(t)$ and $B(t)$ time-dependent), the instantaneous linear growth rate of small infections around the DFE is $c(t) - (\gamma + d)$, where

$$c(t) := \beta V(t)\big(1 - \varepsilon B(t)\big) + \beta_0,$$

and the corresponding instantaneous reproduction potential is $c(t)/(\gamma + d)$. The effective reproduction number including the susceptible fraction is

$$\mathscr{R}_t = \frac{c(t)}{\gamma + d} \cdot \frac{S(t)}{N(t)}.$$

To complement the local stability analysis, we construct an appropriate Lyapunov function to investigate the global dynamics around the disease–free equilibrium.

Theorem 3 (Global stability of the DFE)**.** *Let all parameters be nonnegative and $d > 0$. If $\mathscr{R}_0 \le 1$, then the disease–free equilibrium*

$$x_0 = (S_0, 0, 0, B_0), \qquad S_0 = \frac{\Lambda}{d}, \quad B_0 = \frac{\alpha_0}{\alpha_0 + \eta},$$

of the BC–SIR system is globally asymptotically stable in the feasible region

$$\mathcal{D} = \{(S, I, R, B) : S \ge 0,\ I \ge 0,\ R \ge 0,\ B \in [0, 1]\}.$$

If $\mathscr{R}_0 > 1$, the DFE is unstable.

Proof. Consider the Lyapunov function

$$V(I) = I,$$

which is positive definite with respect to the infected compartment and satisfies $V(I) = 0$ if and only if $I = 0$.

From the infected equation

$$\dot{I} = \lambda(t)S - (\gamma + d)I, \qquad \lambda(t) = \big[\beta V(t)(1 - \varepsilon B(t)) + \beta_0\big]\frac{I}{N},$$

we obtain

$$\dot{V} = \dot{I} = \left(\beta V(t)(1 - \varepsilon B(t)) + \beta_0\right)\frac{S}{N}I - (\gamma + d)I.$$

Since $0 \le S(t) \le N(t)$ and $0 \le B(t) \le 1$ for all $t \ge 0$, it follows that

$$\dot{V} \le \left(\beta \bar{V}(1 - \varepsilon B_0) + \beta_0 - (\gamma + d)\right) I = (\gamma + d)(\mathscr{R}_0 - 1)I.$$

Hence, if $\mathscr{R}_0 \le 1$, then

$$\dot{V} \le 0 \quad \text{in } \mathcal{D},$$

with equality if and only if $I = 0$.

Let

$$\mathcal{E} = \{(S, I, R, B) \in \mathcal{D} : \dot{V} = 0\}.$$

The largest invariant subset of $\mathcal{E}$ is the set $\{I = 0\}$. On this set, the system reduces to

$$\dot{S} = \Lambda - dS + \omega R, \qquad \dot{R} = -(\omega + d)R, \qquad \dot{B} = \alpha_0(1 - B) - \eta B,$$

whose unique equilibrium is $(S, R, B) = (S_0, 0, B_0)$ and is globally asymptotically stable.

By LaSalle's Invariance Principle [26], the disease–free equilibrium x_0 is globally asymptotically stable in $\mathcal{D}$ whenever $\mathscr{R}_0 \leq 1$.

If $\mathscr{R}_0 > 1$, then $\dot{V} > 0$ for I sufficiently small, implying instability of the DFE. □

When $\mathscr{R}_0 > 1$, the system admits a biologically meaningful endemic equilibrium. Its global behavior can be characterized using a Volterra-type Lyapunov function, leading to the following result.

Theorem 4 (Global stability of the endemic equilibrium)**.** *Suppose $V(t) \equiv \bar{V}$ (constant) and all model parameters are nonnegative with $d > 0$. Assume $\mathscr{R}_0 > 1$ so that the endemic equilibrium*

$$x^* = (S^*, I^*, R^*, B^*)$$

exists in the interior of the biologically feasible region

$$\mathcal{D} = \{(S, I, R, B) \in \mathbb{R}^4 : S > 0,\ I > 0,\ R > 0,\ 0 < B \leq 1\}.$$

Then x^* is globally asymptotically stable in $\mathcal{D}$.

Proof. We prove global asymptotic stability by constructing a Lyapunov function of Volterra-type and invoking LaSalle's invariance principle.

Define

$$\mathcal{W}(S, I, R, B) := \Big(S - S^* - S^* \ln \frac{S}{S^*}\Big) + \Big(I - I^* - I^* \ln \frac{I}{I^*}\Big) + \Big(R - R^* - R^* \ln \frac{R}{R^*}\Big) + \Big(B - B^* - B^* \ln \frac{B}{B^*}\Big).$$

Since $x - \xi - \xi \ln(x/\xi) \geq 0$ for $x, \xi > 0$ (with equality iff $x = \xi$), we have $\mathcal{W} \geq 0$ on $\mathcal{D}$, and $\mathcal{W} = 0$ if and only if $(S, I, R, B) = (S^*, I^*, R^*, B^*)$.

Differentiating along trajectories of the system (with $V(t) \equiv \bar{V}$),

$$\dot{\mathcal{W}} = \Big(1 - \frac{S^*}{S}\Big)\dot{S} + \Big(1 - \frac{I^*}{I}\Big)\dot{I} + \Big(1 - \frac{R^*}{R}\Big)\dot{R} + \Big(1 - \frac{B^*}{B}\Big)\dot{B}.$$

Substituting (4)–(7) yields

$$\begin{aligned}\dot{\mathcal{W}} = &\Big(1 - \tfrac{S^*}{S}\Big)\big(\Lambda - \lambda S - dS + \omega R\big) + \Big(1 - \tfrac{I^*}{I}\Big)\big(\lambda S - (\gamma + d)I\big) \\ &+ \Big(1 - \tfrac{R^*}{R}\Big)\big(\gamma I - (\omega + d)R\big) + \Big(1 - \tfrac{B^*}{B}\Big)\big(\alpha_0(1 - B) + \alpha \tfrac{I}{N}(1 - B) - \eta B\big).\end{aligned}$$

At the endemic equilibrium, the steady-state identities imply

$$\lambda^* S^* = (\gamma + d)I^*, \qquad \gamma I^* = (\omega + d)R^*, \qquad \alpha_0(1 - B^*) + \alpha \frac{I^*}{N^*}(1 - B^*) = \eta B^*.$$

Using these identities and standard inequalities, we obtain

$$\dot{\mathcal{W}} \leq -d\frac{(S-S^*)^2}{S} - (\gamma+d)\frac{(I-I^*)^2}{I} - (\omega+d)\frac{(R-R^*)^2}{R} - \eta\frac{(B-B^*)^2}{B}. \tag{13}$$

Thus there exists $\delta > 0$ such that

$$\dot{\mathcal{W}} \leq -\delta\left(\frac{(S-S^*)^2}{S} + \frac{(I-I^*)^2}{I} + \frac{(R-R^*)^2}{R} + \frac{(B-B^*)^2}{B}\right) \leq 0.$$

Moreover, $\dot{\mathcal{W}} = 0$ if and only if

$$S = S^*, \quad I = I^*, \quad R = R^*, \quad B = B^*.$$

Hence the largest invariant subset of $\{\dot{\mathcal{W}} = 0\}$ is the singleton $\{x^*\}$.

By LaSalle's invariance principle, every trajectory in $\mathcal{D}$ converges to x^*. Therefore, the endemic equilibrium is globally asymptotically stable in $\mathcal{D}$. □

4. Sensitivity Analysis of BC-SIR Model

To demonstrate the impact of each parameter on the BC-SIR transmission model, we conducted a sensitivity analysis. To proceed, we used the approach described in the procedure done in, which defined [9] the normalized forward sensitivity index as a variable that varies differently on a parameter Γ, which is defined as follows:

$$\bigcap_{\Gamma}^{\mathscr{R}_0} = \frac{\partial \mathscr{R}_0}{\partial \Gamma}\frac{\Gamma}{\mathscr{R}_0}, \tag{14}$$

where

$$\mathscr{R}_0 = \rho(K) = \frac{\beta\,\bar{V}\,(1-\varepsilon B^*) + \beta_0}{\gamma + d}.$$

Variable	Sensitivity Index Value	Sign
β	0.7012	+
$\bar{V}$	0.7012	+
β_0	0.2987	+
η	0.0136	+
γ	-0.9930	−
ε	-0.0517	−
d	-0.0069	−
α_0	-0.0009	−

Table 2. Values and signs of sensitivity indices for parameters used in the BC-SIR model.

Sensitivity values for all parameters involved in $\mathscr{R}_0$ are shown in the Table (2), and the results are presented in Figure (3).

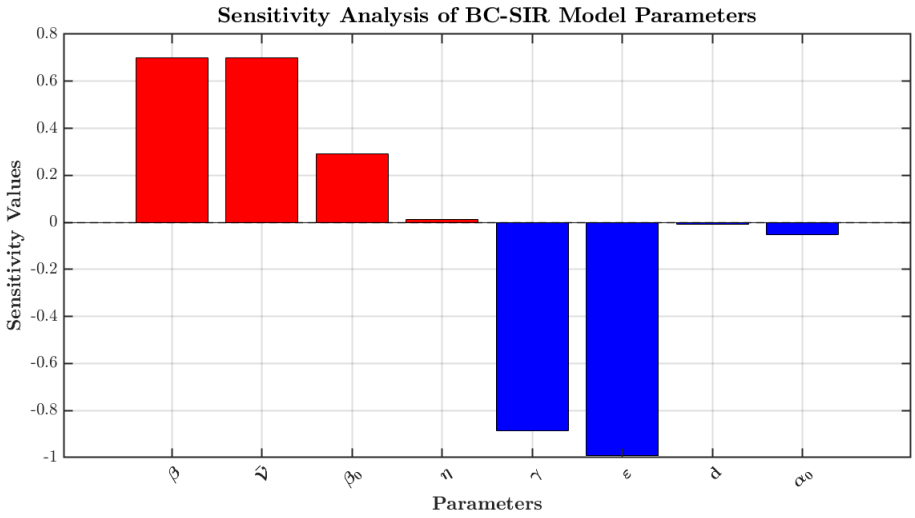

FIGURE 3. BC-SIR Model Sensitivity index.

Using the information from Table (2), we produce a bar graph of the sensitivity levels for each sensitive parameter, where blue indicates negative values and red indicates positive values. The results are displayed in Figure (3). This shows that the parameters β and $\overline{V}$ have positive values and are the most positively sensitive parameters, which implies that R_0 grows as these parameter values increase. However, R_0 decreased as the values of the remaining parameters, γ and ε, increased. These parameters have negative values and are the most sensitive to negative changes.

5. Model Fitting and Parameter Estimation :

This study's approach to parameter estimation combines likelihood-based fitting, numerical simulation using the Runge-Kutta method (RK4) scheme, and compares with observed dengue cases, average temperature, and average rainfall over the 2023 season. First, a fourth-order Runge–Kutta (RK4) method is used to integrate the BC–SIR (Behavior–Climate coupled Susceptible–Infected–Recovered) model with a time-varying climate suitability factor V(t), yielding daily infection incidence data. Next, the model results are evaluated using either synthetic or observed dengue case data. A Poisson maximum likelihood estimation (MLE) approach is used to estimate the parameters $(\beta, \varepsilon, \alpha, \eta)$, which represent transmission rate, behavioral efficacy, risk-driven adoption, and behavioral weariness. The approach minimizes the negative log-likelihood between observed daily cases and model-predicted incidence by conducting a global random search over an ample parameter space, typically involving thousands of random samples. A local coordinate-wise refining step iteratively increases accuracy until

convergence after a promising region has been identified. The underlying model parameters that best suit the epidemic data can be reliably recovered thanks to this hybrid random–local search technique, which guarantees robustness and prevents the optimization from becoming stuck in suboptimal local minima. The plotted graph for the BC-SIR model is shown in Figure (4).

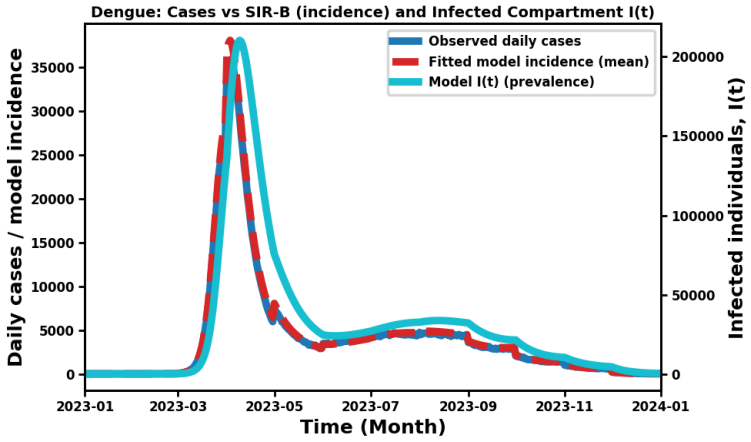

FIGURE 4. BC-SIR model fitted to real data.

5.1. **Numerical Analysis.** In this subsection, we illustrate the numerical simulation of the deterministic BC–SIR model (4)–(7) using the classical fourth–order Runge–Kutta (RK4) method [10]. The BC–SIR model equations are discretized as

$$S_{n+1} = S_n + \frac{\Delta t}{6}\big(k_{1,S} + 2k_{2,S} + 2k_{3,S} + k_{4,S}\big),$$
$$I_{n+1} = I_n + \frac{\Delta t}{6}\big(k_{1,I} + 2k_{2,I} + 2k_{3,I} + k_{4,I}\big),$$
$$R_{n+1} = R_n + \frac{\Delta t}{6}\big(k_{1,R} + 2k_{2,R} + 2k_{3,R} + k_{4,R}\big),$$
$$B_{n+1} = B_n + \frac{\Delta t}{6}\big(k_{1,B} + 2k_{2,B} + 2k_{3,B} + k_{4,B}\big),$$

where $y_n = (S_n, I_n, R_n, B_n)^\top$ and the stage vectors $k_j = (k_{j,S}, k_{j,I}, k_{j,R}, k_{j,B})^\top$ are defined by

$$k_1 = f(t_n, y_n),$$
$$k_2 = f\big(t_n + \tfrac{\Delta t}{2},\, y_n + \tfrac{\Delta t}{2} k_1\big),$$
$$k_3 = f\big(t_n + \tfrac{\Delta t}{2},\, y_n + \tfrac{\Delta t}{2} k_2\big),$$
$$k_4 = f(t_n + \Delta t,\, y_n + \Delta t\, k_3),$$

with

$$k_{j,S} = f_S(t_j, y_j), \quad k_{j,I} = f_I(t_j, y_j), \quad k_{j,R} = f_R(t_j, y_j), \quad k_{j,B} = f_B(t_j, y_j),$$

where f_S, f_I, f_R, f_B denote the right–hand sides of (4)–(7).

Python are used to simulate the BC-SIR system numerically. The fourth-order Runge-Kutta method, an iterative numerical method, was employed to simulate the BC-SIR system, which comprises the state equation and behavioral dynamics as specified in equations 4 to 7. The state system and the behavioral dynamics were solved using the fourth-order Runge-Kutta method. For the simulation, we used the starting conditions $S(0) = 999900$, $I(0) = 100$, $R(0) = 0$, $B(0) = 0.25$, and the parameter values given in Table (1).

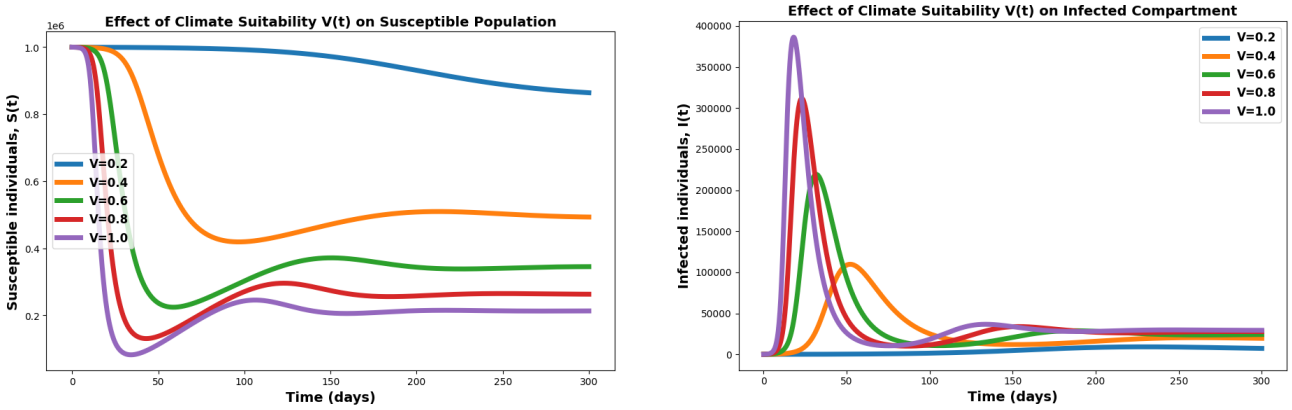

(A) Susceptible population $S(t)$. (B) Infected population $I(t)$.

FIGURE 5. Numerical simulation showing the effect of climate suitability on susceptible and infected populations.

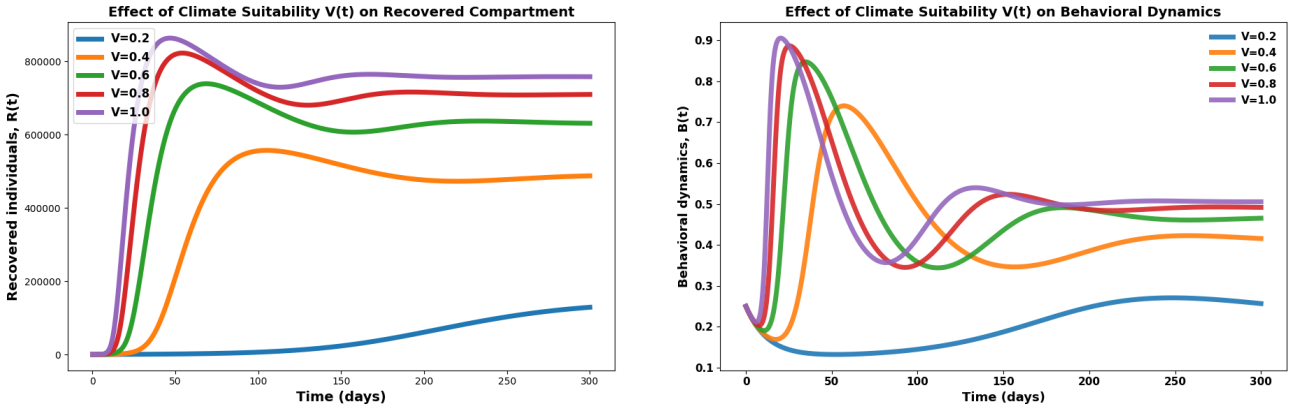

(A) Recovered population $R(t)$. (B) Behavioral compliance $B(t)$.

FIGURE 6. Numerical simulation showing the effect of climate suitability on recovered population and behavioral adaptation.

Under the BC–SIR model, numerical simulations show how climate suitability V(t) affects dengue transmission dynamics. The transmission potential increases as $V(t)$ rises from 0.2 to 1.0. Accordingly, with greater $V(t)$, the susceptible population $S(t)$ drops more steeply, as shown in Figure (5) in the

susceptible individuals compartment, indicating an accelerated depletion of susceptible individuals due to increased infections. By increasing the values of $V(t)$, which leads to a greater and earlier infection peak in the infected compartment $I(t)$, as shown in Figure (5), the infected individuals compartment increases. This reflects the increased mosquito activity and the spread of viruses when the weather is favorable, and the infected population decreases over time. However, when the weather is not favorable for the mosquito population, the spread of viruses tends to stabilize over time. As more people develop temporary immunity, the recovered class $R(t)$ increases more rapidly, achieves higher equilibrium values, and stabilizes over time (see Figure 6 for the compartment of recovered individuals). The population remains susceptible primarily, and the infection is limited to low $V(t)$. Additionally, the behavioral dynamics $B(t)$ increase as $V(t)$ increases, indicating more favorable environmental conditions for the proliferation of mosquitoes, as shown in Figure (6) in the behavioral dynamics compartment. The infection rate is further increased by this growth, which strengthens the positive feedback between the intensity of disease transmission and climate appropriateness. Overall, the findings verify that, despite a gradual decrease in the susceptible population, climatic appropriateness significantly increases transmission intensity, epidemic severity, and the accumulation of recoveries.

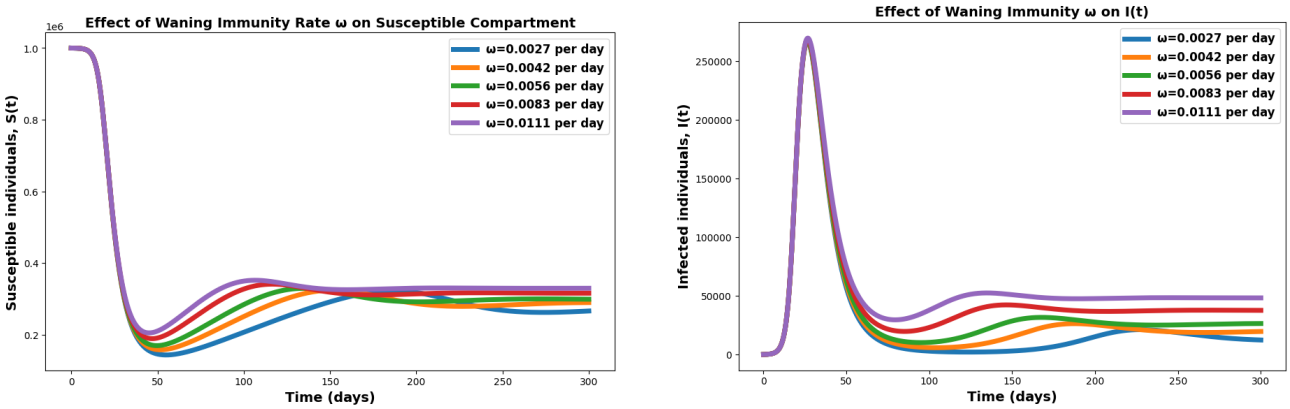

(A) Susceptible population $S(t)$.

(B) Infected population $I(t)$.

FIGURE 7. Numerical simulation of the impact of climate suitability on susceptible and infected populations.

The numerical simulations show how each compartment of the behavior–climate–SIR (BC–SIR) model is affected by the fading immunity rate ω. Higher ω values result in a faster return of recovered individuals to the susceptible class for the susceptible population $S(t)$. As a result, when immunity declines more quickly, $S(t)$ rises over time and stabilizes at a higher equilibrium level as shown in Figure (7), the susceptible individuals compartment. As more susceptibles re-enter the transmission cycle, an increase in ω raises the long-term infection level in the infected compartment $I(t)$. Faster immunity loss maintains chronic, moderate infection levels, as evidenced by the initial sharpness

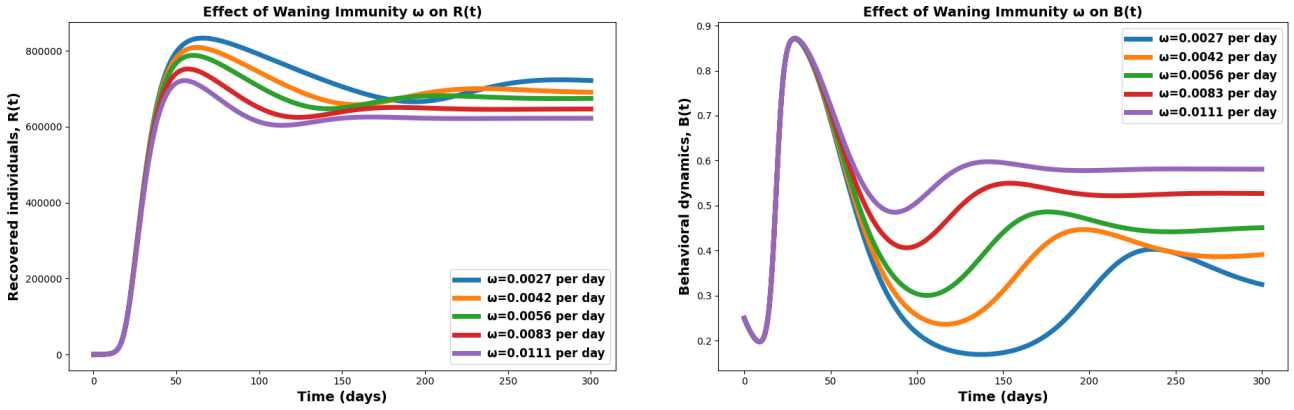

(A) Recovered population $R(t)$. (B) Behavioral compliance $B(t)$.

FIGURE 8. Numerical simulation of the impact of climate suitability on recovered population and behavioral dynamics.

and eventual dampening of the epidemic peaks, as shown in Figure (7), the infected individuals' compartment. In contrast, the recovered population $R(t)$ has a lower steady-state level as ω rises, indicating a quicker return to sensitivity and a shorter lifetime of immunity, see Figure (8), recovered individuals compartment. Finally, the behavioral dynamics $B(t)$ increase with higher ω values, as a higher infection burden maintains stronger public awareness and preventive behavior, as shown in Figure (8), the behavioral dynamics compartment. The system overall transitions from a low to a high endemic equilibrium as ω increases, indicating that shorter immunity durations prolong transmission persistence and strengthen behavioral responses, highlighting the critical role of durable immunity in reducing disease resurgence.

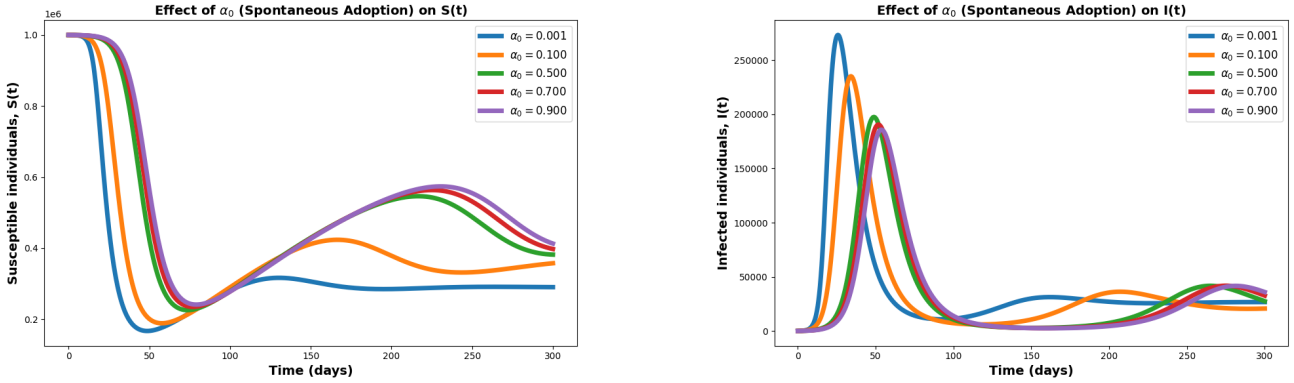

(A) Susceptible population $S(t)$. (B) Infected population $I(t)$.

FIGURE 9. Numerical simulation of the impacts of climate sustainability on susceptible and infected populations.

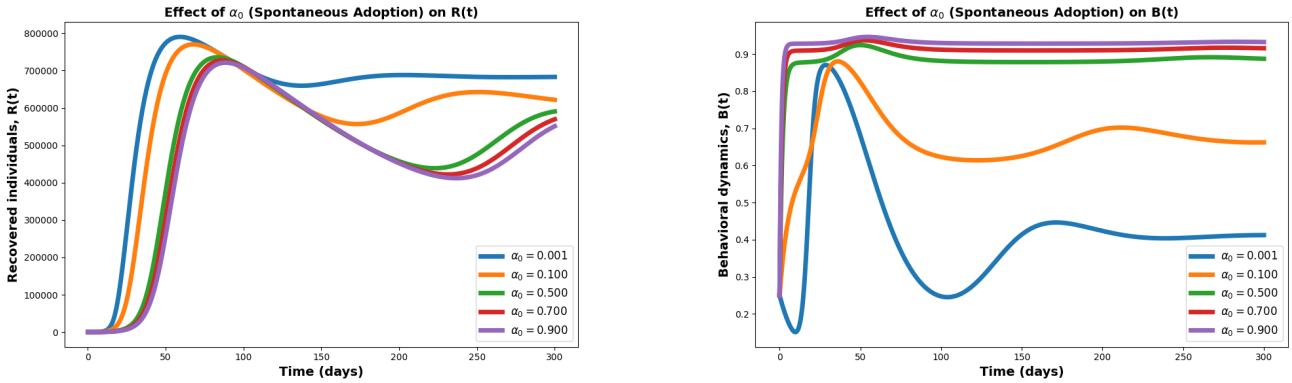

(A) Recovered population $R(t)$.

(B) Behavioral dynamics $B(t)$.

FIGURE 10. Numerical simulation of the impacts of climate sustainability on recovered population and behavioral evolution.

The numerical simulations illustrate the influence of the spontaneous adoption rate α_0 on the dynamics of the behavior–climate SIR (BC–SIR) model. Larger values of α_0, representing stronger awareness-driven or campaign-driven uptake of preventive behaviors, lead to a noticeable reduction in the susceptible population $S(t)$ (see Figure 9). Higher spontaneous compliance limits transmission early, slowing the replenishment of the susceptible class. As α_0 increases, the infected population $I(t)$ correspondingly decreases, producing smaller and shorter epidemic peaks. This occurs because individuals adopt precautionary measures even before direct exposure to infection. Conversely, when α_0 is low, behavioral uptake is weaker, resulting in higher and more prolonged outbreaks (see Figure 9). The recovered population $R(t)$ initially grows more rapidly for smaller α_0 values, due to higher infection incidence, but stabilizes at a comparatively lower level when α_0 is large (Figure 10). Finally, the behavioral compliance level $B(t)$ rises quickly and remains persistently high for larger α_0, indicating sustained engagement in preventive action. When α_0 is small, $B(t)$ evolves more slowly and exhibits delayed or oscillatory behavior (see Figure 10). Overall, increasing α_0 promotes earlier and stronger voluntary behavioral responses, reduces infection severity, and enhances disease control effectiveness. This highlights the importance of proactive public awareness and community education in mitigating dengue transmission.

In the behavior climate SIR (BC–SIR) model, numerical simulations demonstrate how the behavioral fatigue rate (η) influences the overall dynamics of illness. Increasing η lowers behavioral compliance for the susceptible population $S(t)$, which eventually exposes more susceptible people. Due to the prolonged pressure of infection resulting from decreased preventive behavior, $S(t)$ stabilizes at a lower equilibrium as η increases, as shown in Figure (11) for the susceptible population. A higher η is associated with a proportional rise in the infected population, $I(t)$. Intense weariness causes people to stop taking precautions earlier, which in turn raises infection rates and slows the decline

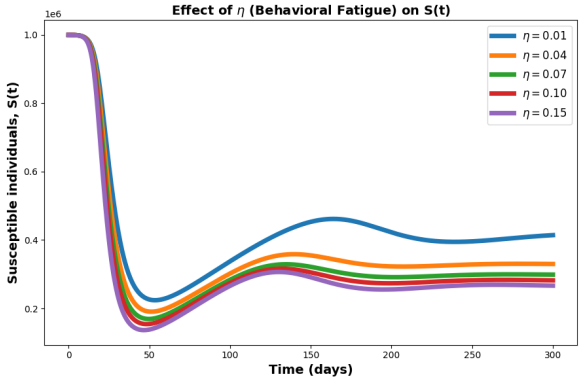

(A) Susceptible population $S(t)$.

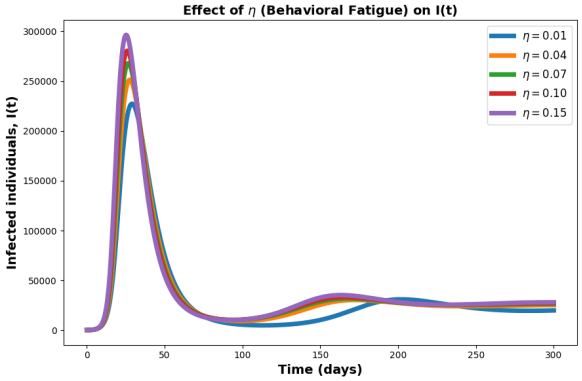

(B) Infected population $I(t)$.

FIGURE 11. Numerical simulation of the impacts of climate sustainability on susceptible and infected populations.

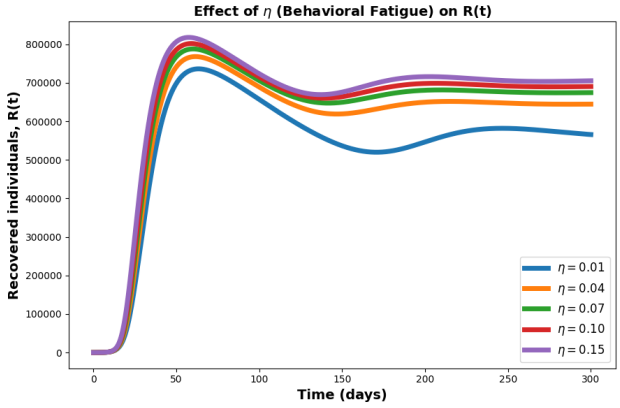

(A) Recovered population $R(t)$.

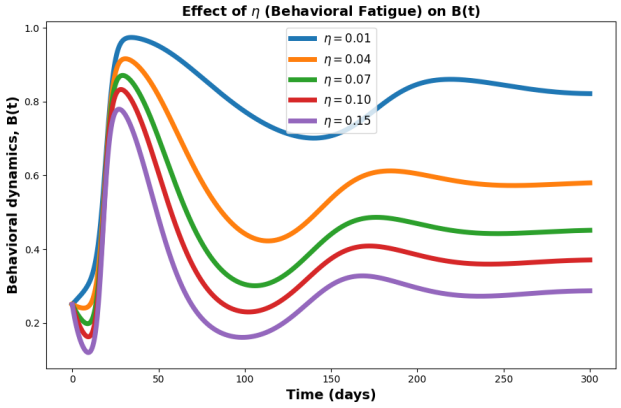

(B) Behavioral dynamics $B(t)$.

FIGURE 12. Numerical simulation of the impacts of climate sustainability on recovered population and behavioral dynamics.

after the epidemic peak. Low η values, on the other hand, sustain greater behavioral protection, which keeps $I(t)$ comparatively lower over time, as seen in Figure (11) for the infected population. The recovered compartment $R(t)$ shows the reverse trend: greater tiredness shortens the duration of immunity. It reduces the total recovered population at equilibrium, whereas lower fatigue (small η) encourages higher recovery peaks, as seen in Figure (12) in the recovered population. η has a direct and vital influence on the behavioral dynamics $B(t)$. Behavioral tiredness causes compliance to decline more rapidly after its initial rise as η increases. Throughout the simulation, populations with small η maintain high $B(t)$ values, whereas populations with large η settle at lower steady states and rapidly decline in their behavioral response, as shown in Figure (12) in the behavioral dynamics. Overall, these findings indicate that increased behavioral fatigue compromises long-term disease control by

prolonging infection persistence and reducing behavioral engagement. This highlights the necessity of ongoing public knowledge and motivation to combat behavioral fatigue during epidemics.

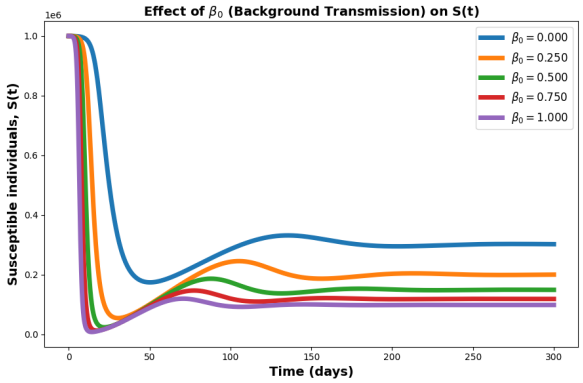

(A) Susceptible population $\mathcal{S}(t)$

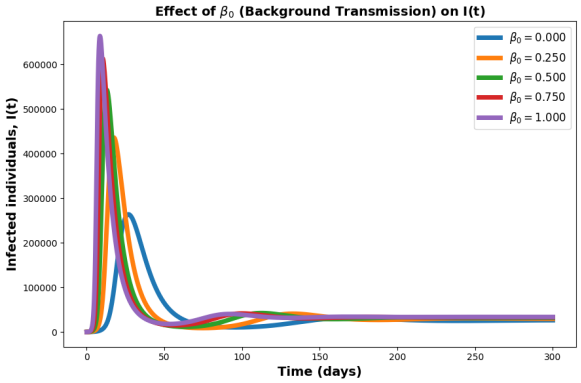

(B) Infected population $\mathcal{I}(t)$

FIGURE 13. Numerical simulation of the impacts of climate sustainability on susceptible and infected populations.

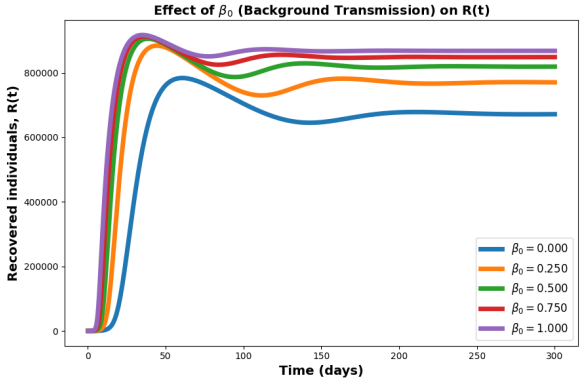

(A) Recovered population $\mathcal{R}(t)$

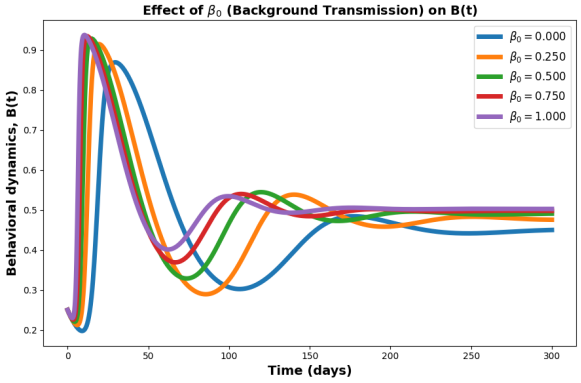

(B) Behavioral dynamics $\mathcal{B}(t)$

FIGURE 14. Numerical simulation of the impacts of climate sustainability on recovered population and behavioral dynamics.

The numerical simulations demonstrate how the system dynamics of the behavior climate SIR (BC–SIR) model are influenced by the background transmission rate (β_0). Higher β_0 values cause the susceptible population $S(t)$ to decline more rapidly because background transmission increases the probability of infection, even in situations where behavioral compliance is strong or climate influences are minimal. As a result, with a greater β_0, $S(t)$ approaches a lower steady-state level as shown in Figure (13) in the susceptible population. With β_0, the infected population $I(t)$ grows dramatically, exhibiting greater and sharper infection peaks. This occurs as a result of increased background transmission, which maintains an ongoing reservoir of infection even during periods of unfavorable climatic conditions,

as seen in Figure (13) in the infected population. As β_0 increases, the recovered population $R(t)$ also increases because more people get infected and then recover. At equilibrium, however, at higher β_0 values, $R(t)$ stabilizes more quickly, suggesting a stronger but shorter epidemic cycle as shown in Figure (14) in the recovered population. There is a noticeable feedback effect in the behavioral dynamics $B(t)$. The behavioral reaction intensifies more rapidly after the initial spike because the perceived danger of infection stays high while β_0 rises. However, as populations continually modify their behavior in response to ongoing infection risk, increased background transmission also causes oscillations in $B(t)$. For larger β_0 values, $B(t)$ converges to a slightly higher equilibrium over time, indicating that continual low-level exposure sustains considerable long-term preventive behavior as seen in Figure (14) in the behavioral dynamics. Overall, the findings indicate that increased background transmission promotes stronger behavioral adaptation, accelerates the early stages of the epidemic, and maintains infection persistence. This emphasizes the significance of lowering baseline transmission sources (such as imported cases or uncontrolled reservoirs) to mitigate disease spread.

Numerical simulations were conducted to investigate the combined effects of climate suitability, $V(t)$, and behavioral compliance, $B(t)$, on dengue transmission dynamics. The model exhibits qualitatively distinct epidemic trajectories depending on the strength and persistence of behavioral responses. Increases in the climate suitability index amplify the force of infection and produce larger epidemic peaks, consistent with the role of temperature and rainfall in enhancing mosquito vector capacity. In contrast, increases in behavioral compliance lead to substantial reductions in both the peak and total number of infections. Variation in the spontaneous behavioral adoption rate α_0 shows that higher values promote an early rise in compliance, which effectively suppresses transmission before infection prevalence becomes large. Consequently, the populations $I(t)$ and $R(t)$ remain comparatively lower over the epidemic duration. When α_0 is small, compliance increases only gradually, allowing sizable outbreaks to occur prior to behavioral adjustment. Similarly, increasing the reactive adoption rate α strengthens the response to observed infection levels, but its effectiveness depends on the timing of disease incidence. The waning parameter η determines the persistence of compliance: larger values yield faster behavioral decay and permit recurrent outbreaks, whereas small values support long-term suppression. Taken together, these results show that climate-driven increases in transmission potential can be substantially mitigated by sufficiently strong and sustained behavioral adoption, particularly when preventive behavior is established preemptively rather than reactively.

The integration of climate suitability and behavioral adaptation provides a more comprehensive representation of dengue transmission dynamics compared to standard SIR models. The simulations indicate that climatic conditions, while influential, do not determine epidemic magnitude in isolation; rather, the population's behavioral response critically modulates the realized transmission intensity. This aligns with empirical evidence that the interaction between environmental conditions and human

protective behavior shapes dengue outbreaks. The results underscore the importance of spontaneous adoption of preventive measures. When individuals adopt protective behaviors due to public health messaging or general awareness (captured by α_0), compliance increases before disease burden rises, reducing the effective reproduction number $\mathcal{R}_t$ throughout the epidemic. Reactive adoption alone (α) is insufficient if it occurs only after transmission has accelerated. Furthermore, behavioral fatigue (η) emerges as a key factor governing long-term disease dynamics: if compliance cannot be sustained, the system is prone to resurgence even following periods of control. These findings suggest that public health interventions should prioritize early-season awareness campaigns, continuous risk communication, and support for sustained behavioral adherence, particularly in settings where climatic conditions favor the proliferation of vectors.

6. Conclusion

This study presented a behavior–climate coupled SIR model for dengue transmission, incorporating adaptive behavioral dynamics and climate-driven modulation of transmission rates. The analysis demonstrates that while favorable climatic conditions increase transmission potential, proactive and sustained behavioral compliance can significantly mitigate disease spread. In particular, spontaneous behavioral adoption plays a central role in preventing large outbreaks, whereas reactive adjustments alone are insufficient to achieve lasting control. The results highlight the need for integrated public health strategies that jointly consider environmental conditions and human behavior. Effective dengue control requires not only vector surveillance and climatic monitoring but also early and sustained community engagement efforts aimed at promoting long-term adherence to preventive practices. This framework provides a basis for future work on optimal intervention timing, control strategy evaluation, and data-informed estimation of time-varying transmission and compliance parameters in dengue-endemic regions.

Acknowledgement. The authors would like to thank the anonymous reviewers for their careful evaluation and constructive comments, which substantially improved the scientific quality of this manuscript.

Authors' Contributions. All authors have read and approved the final version of the manuscript. The authors contributed equally to this work.

Conflict of Interest. The authors declare that there are no conflicts of interest regarding the publication of this paper.

References

[1] M. Aguiar, V. Anam, K.B. Blyuss, C.D.S. Estadilla, B.V. Guerrero, et al., Mathematical Models for Dengue Fever Epidemiology: A 10-Year Systematic Review, Phys. Life Rev. 40 (2022), 65–92. https://doi.org/10.1016/j.plrev.2022.02.001.

[2] M. Al Mobin, M. Kamrujjaman, M.M. Molla, S. Chen, Analysis of a Data-Driven Vector-Borne Dengue Transmission Model for a Tropical Environment in Bangladesh, Int. J. Differ. Equ. 2024 (2024), 2959770. https://doi.org/10.1155/2024/2959770.

[3] W.M. Alobuia, C. Missikpode, M. Aung, P.E. Jolly, Knowledge, Attitude, and Practices Regarding Vector-Borne Diseases in Western Jamaica, Ann. Glob. Health 81 (2016), 654. https://doi.org/10.1016/j.aogh.2015.08.013.

[4] K.E. Alam, M.J. Ahmed, R. Chalise, M.A. Rahman, T.T. Mathin, et al., Time Series Analysis of Dengue Incidence and Its Association with Meteorological Risk Factors in Bangladesh, PLOS One 20 (2025), e0323238. https://doi.org/10.1371/journal.pone.0323238.

[5] R.M. Anderson, R.M. May, Infectious Diseases of Humans: Dynamics and Control, Oxford University Press, 1991.

[6] R. Banik, M.S. Islam, M. Mubarak, M. Rahman, H.A. Gesesew, et al., Public Knowledge, Belief, and Preventive Practices Regarding Dengue: Findings from a Community-Based Survey in Rural Bangladesh, PLOS Neglected Trop. Dis. 17 (2023), e0011778. https://doi.org/10.1371/journal.pntd.0011778.

[7] C. Betsch, L. Korn, P. Sprengholz, L. Felgendreff, S. Eitze, et al., Social and Behavioral Consequences of Mask Policies during the COVID-19 Pandemic, Proc. Natl. Acad. Sci. USA 117 (2020), 21851–21853. https://doi.org/10.1073/pnas.2011674117.

[8] S. Bhatt, P.W. Gething, O.J. Brady, J.P. Messina, A.W. Farlow, et al., The Global Distribution and Burden of Dengue, Nature 496 (2013), 504–507. https://doi.org/10.1038/nature12060.

[9] S.M. Blower, H. Dowlatabadi, Sensitivity and Uncertainty Analysis of Complex Models of Disease Transmission: An HIV Model, as an Example, Int. Stat. Rev. / Rev. Int. Stat. 62 (1994), 229–243. https://doi.org/10.2307/1403510.

[10] J.C. Butcher, Numerical Methods for Ordinary Differential Equations, Wiley, 2016. https://doi.org/10.1002/9781119121534.

[11] C. Caminade, K.M. McIntyre, A.E. Jones, Impact of Recent and Future Climate Change on Vector-borne Diseases, Ann. N. Y. Acad. Sci. 1436 (2018), 157–173. https://doi.org/10.1111/nyas.13950.

[12] V. Capasso, G. Serio, A Generalization of the Kermack-Mckendrick Deterministic Epidemic Model, Math. Biosci. 42 (1978), 43–61. https://doi.org/10.1016/0025-5564(78)90006-8.

[13] C. Carreto, R. Gutiérrez-Romero, T. Rodríguez, Climate-Driven Mosquito-Borne Viral Suitability Index: Measuring Risk Transmission of Dengue, Chikungunya and Zika in Mexico, Int. J. Health Geogr. 21 (2022), 15. https://doi.org/10.1186/s12942-022-00317-0.

[14] A. Cori, N.M. Ferguson, C. Fraser, S. Cauchemez, A New Framework and Software to Estimate Time-Varying Reproduction Numbers during Epidemics, Am. J. Epidemiol. 178 (2013), 1505–1512. https://doi.org/10.1093/aje/kwt133.

[15] A. d'Onofrio, P. Manfredi, E. Salinelli, Vaccinating Behaviour, Information, and the Dynamics of SIR Vaccine Preventable Diseases, Theor. Popul. Biol. 71 (2007), 301–317. https://doi.org/10.1016/j.tpb.2007.01.001.

[16] E.P. Fenichel, C. Castillo-Chavez, M.G. Ceddia, G. Chowell, P.A.G. Parra, et al., Adaptive Human Behavior in Epidemiological Models, Proc. Natl. Acad. Sci. 108 (2011), 6306–6311. https://doi.org/10.1073/pnas.1011250108.

[17] S. Funk, M. Salathé, V.A.A. Jansen, Modelling the Influence of Human Behaviour on the Spread of Infectious Diseases: A Review, J. R. Soc. Interface 7 (2010), 1247–1256. https://doi.org/10.1098/rsif.2010.0142.

[18] A. Gasparrini, B. Armstrong, M.G. Kenward, Distributed Lag Non-linear Models, Stat. Med. 29 (2010), 2224–2234. https://doi.org/10.1002/sim.3940.

[19] M.I. Hossain, N.E. Alam, S. Akter, U. Suriea, S. Aktar, et al., Knowledge, Awareness and Preventive Practices of Dengue Outbreak in Bangladesh: A Countrywide Study, PLOS ONE 16 (2021), e0252852. https://doi.org/10.1371/journal.pone.0252852.

[20] S. Hossain, M.M. Islam, M.A. Hasan, P.B. Chowdhury, I.A. Easty, et al., Association of Climate Factors with Dengue Incidence in Bangladesh, Dhaka City: A Count Regression Approach, Heliyon 9 (2023), e16053. https://doi.org/10.1016/j.heliyon.2023.e16053.

[21] S. Islam, C.E. Haque, S. Hossain, J. Hanesiak, Climate Variability, Dengue Vector Abundance and Dengue Fever Cases in Dhaka, Bangladesh: A Time-Series Study, Atmosphere 12 (2021), 905. https://doi.org/10.3390/atmos12070905.

[22] M.S. Islam, P. Shahrear, G. Saha, M. Ataullha, M.S. Rahman, Mathematical Analysis and Prediction of Future Outbreak of Dengue on Time-Varying Contact Rate Using Machine Learning Approach, Comput. Biol. Med. 178 (2024), 108707. https://doi.org/10.1016/j.compbiomed.2024.108707.

[23] M.A. Johansson, F. Dominici, G.E. Glass, Local and Global Effects of Climate on Dengue Transmission in Puerto Rico, PLoS Neglected Trop. Dis. 3 (2009), e382. https://doi.org/10.1371/journal.pntd.0000382.

[24] R. Nigam, Climatic Factors Influencing Dengue Cases in Bhopal City: A Model for Dengue Prediction, Int. J. Infect. Dis. 73 (2018), 197. https://doi.org/10.1016/j.ijid.2018.04.3862.

[25] S.M. Kissler, C. Tedijanto, E. Goldstein, Y.H. Grad, M. Lipsitch, Projecting the Transmission Dynamics of SARS-Cov-2 Through the Postpandemic Period, Science 368 (2020), 860–868. https://doi.org/10.1126/science.abb5793.

[26] J.P. LaSalle, The Stability of Dynamical Systems, SIAM, Philadelphia, 1976.

[27] K. Liu, X. Hou, Z. Ren, R. Lowe, Y. Wang, et al., Climate Factors and the East Asian Summer Monsoon May Drive Large Outbreaks of Dengue in China, Environ. Res. 183 (2020), 109190. https://doi.org/10.1016/j.envres.2020.109190.

[28] J.P. Messina, O.J. Brady, N. Golding, M.U.G. Kraemer, G.R.W. Wint, et al., The Current and Future Global Distribution and Population at Risk of Dengue, Nat. Microbiol. 4 (2019), 1508–1515. https://doi.org/10.1038/s41564-019-0476-8.

[29] E.A. Mordecai, J.M. Cohen, M.V. Evans, P. Gudapati, L.R. Johnson, et al., Detecting the Impact of Temperature on Transmission of Zika, Dengue, and Chikungunya Using Mechanistic Models, PLOS Neglected Trop. Dis. 11 (2017), e0005568. https://doi.org/10.1371/journal.pntd.0005568.

[30] S. Naish, P. Dale, J.S. Mackenzie, J. McBride, K. Mengersen, et al., Climate Change and Dengue: A Critical and Systematic Review of Quantitative Modelling Approaches, BMC Infect. Dis. 14 (2014), 167. https://doi.org/10.1186/1471-2334-14-167.

[31] S. Naher, F. Rabbi, M.M. Hossain, R. Banik, S. Pervez, et al., Forecasting the Incidence of Dengue in Bangladesh—Application of Time Series Model, Health Sci. Rep. 5 (2022), e666. https://doi.org/10.1002/hsr2.666.

[32] A. Pandey, A. Mubayi, J. Medlock, Comparing Vector–Host and SIR Models for Dengue Transmission, Math. Biosci. 246 (2013), 252–259. https://doi.org/10.1016/j.mbs.2013.10.007.

[33] K. Hossain, S. Chowdhury, I.S. Shanta, M.S. Hossain, P.K. Ghosh, et al., Spatio-Temporal Patterns of Dengue in Bangladesh during 2019 to 2023: Implications for Targeted Control Strategies, PLOS Neglected Trop. Dis. 18 (2024), e0012503. https://doi.org/10.1371/journal.pntd.0012503.

[34] P. Poletti, M. Ajelli, S. Merler, The Effect of Risk Perception on the 2009 H1N1 Pandemic Influenza Dynamics, PLoS ONE 6 (2011), e16460. https://doi.org/10.1371/journal.pone.0016460.

[35] M.S. Rahman, M.A.B. Shiddik, Explainable Artificial Intelligence for Predicting Dengue Outbreaks in Bangladesh Using Eco-Climatic Triggers, Glob. Epidemiol. 10 (2025), 100210. https://doi.org/10.1016/j.gloepi.2025.100210.

[36] M.A. Robert, R.C. Christofferson, P.D. Weber, H.J. Wearing, Temperature Impacts on Dengue Emergence in the United States: Investigating the Role of Seasonality and Climate Change, Epidemics 28 (2019), 100344. https://doi.org/10.1016/j.epidem.2019.05.003.

[37] I. Sarker, M.R. Karim, S. E-Barket, M. Hasan, Dengue Fever Mapping in Bangladesh: A Spatial Modeling Approach, Health Sci. Rep. 7 (2024), e2154. https://doi.org/10.1002/hsr2.2154.

[38] A.S. Siraj, R.J. Oidtman, J.H. Huber, M.U.G. Kraemer, O.J. Brady, et al., Temperature Modulates Dengue Virus Epidemic Growth Rates Through Its Effects on Reproduction Numbers and Generation Intervals, PLOS Neglected Trop. Dis. 11 (2017), e0005797. https://doi.org/10.1371/journal.pntd.0005797.

[39] P. van den Driessche, J. Watmough, Reproduction Numbers and Sub-Threshold Endemic Equilibria for Compartmental Models of Disease Transmission, Math. Biosci. 180 (2002), 29–48. https://doi.org/10.1016/s0025-5564(02)00108-6.

[40] J. Wallinga, Different Epidemic Curves for Severe Acute Respiratory Syndrome Reveal Similar Impacts of Control Measures, Am. J. Epidemiol. 160 (2004), 509–516. https://doi.org/10.1093/aje/kwh255.

[41] World Bank, Birth Rate, Crude (Per 1,000 People) – Bangladesh, World Bank Data, 2023. https://data.worldbank.org/indicator/SP.DYN.CBRT.IN?locations=BD.

[42] World Bank, Population, Total – Bangladesh, World Bank Data, 2023. https://data.worldbank.org/indicator/SP.POP.TOTL?locations=BD.

[43] World Health Organization, Dengue and Severe Dengue, https://www.who.int/health-topics/dengue-and-severe-dengue.

[44] C. Xu, J. Xu, L. Wang, Long-Term Effects of Climate Factors on Dengue Fever Over a 40-Year Period, BMC Public Health 24 (2024), 1451. https://doi.org/10.1186/s12889-024-18869-0.

[45] T.K. Yamana, S. Kandula, J. Shaman, Superensemble Forecasts of Dengue Outbreaks, J. R. Soc. Interface 13 (2016), 20160410. https://doi.org/10.1098/rsif.2016.0410.

[46] Q. Zeng, X. Yu, H. Ni, L. Xiao, T. Xu, et al., Dengue Transmission Dynamics Prediction by Combining Metapopulation Networks and Kalman Filter Algorithm, PLOS Neglected Trop. Dis. 17 (2023), e0011418. https://doi.org/10.1371/journal.pntd.0011418.